

Oleg V. Prezhdo

Quantized hamilton dynamics

Received: 2 April 2005 / Accepted: 28 September 2005
© Springer-Verlag 2005

Abstract The paper describes the quantized Hamilton dynamics (QHD) approach that extends classical Hamiltonian dynamics and captures quantum effects, such as zero point energy, tunneling, decoherence, branching, and state-specific dynamics. The approximations are made by closures of the hierarchy of Heisenberg equations for quantum observables with the higher order observables decomposed into products of the lower order ones. The technique is applied to the vibrational energy exchange in a water molecule, the tunneling escape from a metastable state, the double-slit interference, the population transfer, dephasing and vibrational coherence transfer in a two-level system coupled to a phonon, and the scattering of a light particle off a surface phonon, where QHD is coupled to quantum mechanics in the Schrödinger representation. Generation of thermal ensembles in the extended space of QHD variables is discussed. QHD reduces to classical mechanics at the first order, closely resembles classical mechanics at the higher orders, and requires little computational effort, providing an efficient tool for treatment of the quantum effects in large systems.

Keywords Semiclassical dynamics · Closure · Heisenberg representation · Extended phase space · Gaussians

1 Introduction

Chemical reaction dynamics [1,2] is concerned with the intricate details of breaking and forming chemical bonds. To understand the outcome of a particular reaction the chemist pictures the molecular structures of reactants and products. Next, a hypothesis regarding the reaction mechanism is developed using the notion of a transition state (TS) as the single most important configuration marking the reactant–product boundary. The idea of a reaction dynamics bottleneck pro-

vided by the TS is at the heart of the TS theories [3]. The reaction rates that follow from the TS theories provide a limited description averaged over various encounters, orientations and relative velocities of the reactants, all possible pathways from reactants to products, etc. Multiple TSs are possible and often cannot be determined a priori without a careful analysis of the potential energy surfaces, particularly in multiple dimensions [4,5]. Direct simulation of chemical dynamics provides a conceptually simpler alternative and a more detailed picture of chemical processes.

The chemical applications of lasers [1,6] have generated additional interest in reaction dynamics. Many of the old reactions have been re-examined by the time-resolved optical and scattering techniques with unprecedented temporal and structural detail. Novel phenomena have been discovered and require theoretical modeling. The available temporal resolution spans all chemical scales from slow macroscopic transformations to sub-picosecond electronic rearrangements. Novel types of chemical reactions are emerging involving mesoscopic and nanosize objects that cannot be described by macroscopic thermodynamics, emphasizing dynamical and quantum effects. Single molecule experiments [7] avoid ensemble averaging and allow one to follow individual reaction events in much the same way as one would a trajectory on a computer.

The many-body dynamics of chemical reactions are typically too complicated for a fully quantum mechanical analysis. Although considerable progress has been made in the development of exact quantum-mechanical methods, [8, 9], they are still only applicable to relatively small molecular systems. In contrast, classical-dynamics methods are routinely used to study complex chemical problems involving many thousands of particles [10, 11]. Quantum effects such as zero point energy, tunneling, dephasing, interference, branching, etc. are essential in chemistry, and cannot be avoided in the time-resolved studies involving light-matter interaction. One is, therefore, necessarily interested in approaches that capture the quantum phenomena in many degrees of freedom. A number of such approaches involving semiclassical and mixed quantum–classical dynamics have been proposed

O. V. Prezhdo
Department of Chemistry,
University of Washington,
Seattle, WA 98195-1700, USA
E-mail: prezhdo@u.washington.edu

and applied in recent years, and remain under active development [12–50].

The great utility of the semiclassical and quantum–classical dynamics can be illustrated with numerous examples from most chemistry disciplines. For example, Rossky and co-workers [12–18] have applied the stationary-phase surface-hopping approach to investigate the non-radiative relaxation of solvated electrons. They successfully elucidated the origin of the electronic spectra and relaxation timescales observed in various solvents [12, 13, 17] the types of solvent vibrational modes involved in promoting the relaxation and accepting the excess electronic energy [14, 18] and the absence of the solvent isotope effect [15, 16]. Tully and co-workers [19–21] have studied the chemical dynamics at metal surfaces using molecular dynamics with electronic friction, and established the electron and phonon mechanisms of vibrational relaxation of molecular adsorbates. Miller and co-workers have derived a number of semiclassical expressions for the thermal rate constants [22, 23] and applied them to study proton transfer in a polar solvent [24] atom abstraction in molecular collisions [25, 26] dynamics of alkane hydroxylation in methane monooxygenase [27], and other reactions. Heller and co-workers [28, 29] have described quantum corals, mirages and two-dimensional electron flows with semiclassical dynamics. Many quantum control phenomena have been investigated semiclassically, including the proton transfer in large molecular systems with strong decoherence by Batista and Brumer [30], the Trojan states in hydrogen by Shapiro et al. [31], I_2 in solid matrices by the groups of Wyatt [32] and Coker [33], and the wave-packet interferometry by Cina [34]. Voth and co-workers have incorporated quantum statistics into centroid molecular dynamics [35] and modeled para-hydrogen and ortho-deuterium [36]. The proton and hydride transfer reactions in biological systems have been thoroughly described with the quantum–classical dynamics by Karplus [37], Truhlar [38], Hammes-Schiffer [39] and others. Using dissipative multilevel electronic dynamics Bittner has investigated energy relaxation in organic light-emitting diodes, elucidating the universal scaling laws [40] and the spin dependence of the electron–hole capture kinetics [41]. Our group [42–50] has used mixed quantum–classical density functional theory in order to resolve the controversy regarding the mechanism of the ultrafast photoinduced electron injection in the Grätzel solar cell, proposing a means for increasing the solar cell voltage [46]. Many other outstanding applications of the semiclassical and quantum–classical dynamics may be found in the literature.

Driven by novel types of problems and mathematical elegance, several new directions in semiclassical dynamics have originated recently [51–91]. Under investigation are methods of mixing different levels of theory – in particular quantum and classical mechanics – as well as efficient hierarchies of approximations to bridge the two. The new ideas are deeply rooted in the earlier work. Semiclassical theory in the WKB (Wigner–Kramers–Brillouin) sense has emerged as a powerful computational tool, owing to the initial value representation (IVR), which casts the numerically

difficult problem of integrating over classical trajectories subject to both initial and final boundary conditions to the much simpler problem of generating ensembles of trajectories with initial positions and momenta [22, 51]. The coherent wave-packet representation has been used to construct a semiclassical propagator [52]. The quantum-dressed dynamics [53], the multiple-spawning approach [54, 55] and the Hamiltonian formulation of quantum mechanics [56] converge to the quantum results. The formal quantum–classical Lie algebraic connection is being investigated, including the Wigner density [57] and the partial Wigner transform schemes [58–61].

The revived interest in the interpretation of quantum mechanics has been taken to a practical level. The de-Broglie–Bohm, or hydrodynamic, formulation of quantum mechanics provides a very intuitive picture, where an ensemble of particles flowing along classical-like trajectories are entangled through a non-local interaction. The hydrodynamic formulation provides a solution to the quantum backreaction problem in mixed quantum–classical mechanics [62] and gives numerical tools for solving the time-dependent Schrödinger equation [63–68]. The decoherent histories interpretation of quantum mechanics explains the transition from the microscopic quantum laws to the macroscopically observed classical behavior, giving rise to stochastic wave-function approaches [69–71] that focus on a small subsystem and approximate the remaining majority as a quantum bath, thereby dramatically simplifying the problem. Quantum noise has been added to the explicit classical treatment of the environment in the mean-field of the stochastic Schrödinger equation [72].

Non-adiabatic molecular dynamics (NAMD) constitutes an important class of semiclassical approximations and is particularly valuable for modeling laser-induced processes where heavy, nearly-classical nuclei slowly respond to the photoinduced ultrafast dynamics of quantum electrons and induce nonradiative relaxation. Developed originally for gas-phase atomic and molecular collisions, NAMD has been expanded to treat condensed matter. The recent advances in NAMD are associated with descriptions of extended NA coupling regions by fewest-switches surface-hopping [73, 74] decoherence in the quantum subsystem [72, 75–77], branching of classical trajectories due to decoherence [72, 77] the combination of discrete and continuous quantum states [78], the optimal choice of classical trajectories by stationary-phase surface-hopping [79] and mean-field with surface-hopping [80].

The present article describes the quantized Hamilton dynamics (QHD) approach that is under development in our group [81–91]. Its features include direct focus on the observables, the creation of reduced models for the quantum effects, flexibility in the approximation levels and dynamical variables, and a simple quantum–classical connection. The approximations are derived for the evolution of relevant expectation values in the Heisenberg representation without an attempt to reconstruct the full quantum wave function or density matrix. The QHD equations are very similar to the classical Hamilton equations, to which they compare in

computational effort. Many of the standard numerical tools of classical molecular dynamics can be applied to QHD, facilitating its implementation and applications.

2 The closure approximation

The QHD approach provides a hierarchy of approximations to quantum mechanics in the Heisenberg representation. Application of the Heisenberg equation of motion (EOM)

$$i\hbar \frac{d}{dt} \langle \hat{A} \rangle = \langle [\hat{H}, \hat{A}] \rangle \quad (1)$$

to a system observable $\langle \hat{A} \rangle$ of interest (where the brackets denote the quantum average over the initial state) results in a chain of equations, where the original operator becomes coupled to higher order operators. Apart from the rare exceptions, such as the harmonic oscillator and spin systems in which quantum dynamics can be described exactly by a finite set of operators, the Heisenberg EOM form an infinite chain. The QHD approximations are obtained by terminating the chain with a closure that expresses the expectation values of the higher order operators in terms of products of the expectation values of the lower order operators. Such closures are often used in many-particle theories of quantum [92–94] and statistical [95–97] mechanics. The approximation of all expectation values by products of the first order expectations of position and momentum reduces the quantum Heisenberg EOM to the Hamilton EOM of classical mechanics. A non-trivial approximation appears in the second order, where the cubic and higher order expectation values are decomposed into the linear and quadratic terms. For instance, the approximation

$$\langle ABC \rangle \approx \langle AB \rangle \langle C \rangle + \langle AC \rangle \langle B \rangle + \langle BC \rangle \langle A \rangle - 2\langle A \rangle \langle B \rangle \langle C \rangle \quad (2)$$

for the cubic term is obtained by first extracting

$$\begin{aligned} \langle ABC \rangle &= \langle (A - \langle A \rangle + \langle A \rangle) (B - \langle B \rangle + \langle B \rangle) (C - \langle C \rangle + \langle C \rangle) \rangle \\ &= \langle (A - \langle A \rangle) (B - \langle B \rangle) (C - \langle C \rangle) \rangle \\ &\quad + \langle AB \rangle \langle C \rangle + \langle AC \rangle \langle B \rangle + \langle BC \rangle \langle A \rangle - 2\langle A \rangle \langle B \rangle \langle C \rangle \end{aligned} \quad (3)$$

and then decomposing the irreducible part into all possible pairings of lower order terms, as in Wick's theorem [92]

$$\begin{aligned} \langle (A - \langle A \rangle) (B - \langle B \rangle) (C - \langle C \rangle) \rangle &\approx \langle (A - \langle A \rangle) (B - \langle B \rangle) \rangle \langle (C - \langle C \rangle) \rangle \\ &\quad + \langle (A - \langle A \rangle) (C - \langle C \rangle) \rangle \langle (B - \langle B \rangle) \rangle \\ &\quad + \langle (B - \langle B \rangle) (C - \langle C \rangle) \rangle \langle (A - \langle A \rangle) \rangle \\ &= 0. \end{aligned} \quad (4)$$

Explicit decompositions of the fourth and fifth order terms can be found in [81] and [84], respectively.

For instance, the Heisenberg hierarchy generated starting with \hat{Q} for the cubic potential

$$V(\hat{Q}) = \frac{\hat{Q}^2}{2!} + \frac{\hat{Q}^3}{3!}. \quad (5)$$

reads

$$\begin{aligned} \frac{d\langle \hat{Q} \rangle}{dt} &= \langle \hat{P} \rangle, \quad \frac{d\langle \hat{P} \rangle}{dt} = -\langle \hat{Q} \rangle - \frac{\langle \hat{Q}^2 \rangle}{2} \\ \frac{d\langle \hat{Q}^2 \rangle}{dt} &= \langle \hat{P} \hat{Q} + \hat{Q} \hat{P} \rangle \equiv 2\langle \hat{P} \hat{Q} \rangle_s \\ \frac{d\langle \hat{P} \hat{Q} \rangle_s}{dt} &= \langle \hat{P}^2 \rangle - \langle \hat{Q}^2 \rangle - \frac{\langle \hat{Q}^3 \rangle}{2} \\ \frac{d\langle \hat{P}^2 \rangle_s}{dt} &= -2\langle \hat{P} \hat{Q} \rangle_s - \langle \hat{P} \hat{Q}^2 \rangle_s. \end{aligned} \quad (6)$$

In order to terminate the hierarchy, the $\langle \hat{Q}^3 \rangle$ and $\langle \hat{P} \hat{Q}^2 \rangle_s$ terms are decomposed using the closure (2). Apart from the operator ordering these equations are identical with the corresponding classical equations. The first order closure provides the correct classical limit. Truncation rather than decomposition of the higher order terms results in simpler, linear differential equations, but does not give the classical limit. The second order closure is equivalent to the Gaussian approximation. The closure is accurate at short times, since the low order expectation values do not immediately experience the changes in the higher order terms several equations down the chain. In addition, the closure reproduces the global quantum features, for instance, preserves zero point energy (ZPE) at all times, describes tunneling, dephasing, branching, etc.

It is interesting to note that the initial motivation for the QHD formalism [81] arose from consideration of the quantum–classical Lie brackets and an attempt to define a bracket

$$\begin{aligned} \frac{\partial \langle A(\hat{P}, \hat{Q}) \rangle}{\partial t} &= \frac{i}{\hbar} \langle [A(\hat{P}, \hat{Q}), H_0(\hat{P}, \hat{Q})] \rangle \\ &\quad + \langle \{A(\langle \hat{P} \rangle, \langle \hat{Q} \rangle), H_1(\langle \hat{P} \rangle, \langle \hat{Q} \rangle)\} \rangle. \end{aligned} \quad (7)$$

by splitting the total Hamiltonian into a quantum H_0 and classical H_1 parts and applying the Heisenberg commutator and the Poisson bracket respectively. The formal and practical features of this construction deserve further investigation.

The variables used in the QHD approach depend on the specific problem under study. The examples considered below apply the closure approximation to the moments of the classical-like position and momentum operators, the mean-field coupling of these moments to a quantum system described by a wavefunction, and the spin–phonon operators.

3 QHD equations for moments of P and Q

The most common Hamiltonian is a function of the position \hat{Q} and momentum \hat{P} operators

$$H(\hat{P}, \hat{Q}) = \frac{\hat{P}^2}{2m} + V(\hat{Q}). \quad (8)$$

The potential $V(\hat{Q})$ is Taylor expanded around the average $\langle \hat{Q} \rangle \equiv q$

$$V(\hat{Q}) \approx V(q) + \sum_{k=1}^n \frac{1}{k!} V^{(k)}(q) (\hat{Q} - q)^k. \quad (9)$$

The potential energy operator and its derivatives directly can also be treated as QHD variables directly. For potentials containing cubic or higher order terms, the Heisenberg EOM (1) initiates an infinite hierarchy of equations involving increasing orders of \hat{P} and \hat{Q} . While higher order QHDs have been derived and converge to the exact results [84], the second order QHD for \hat{P} and \hat{Q} is of particular interest. It is the simplest extension of classical mechanics that captures ZPE and moderate tunneling. The widely used Gaussian approximations [98–102] constitute special cases of QHD-2. With the first-order closure for the coupling between different degrees of freedom, QHD-2 can be mapped onto classical mechanics. The mapping facilitates both implementation and interpretation of the second order dynamics.

3.1 Classical mapping for the second order QHD

In addition to the classical-like $\langle \hat{Q} \rangle$, $\langle \hat{P} \rangle$, the second order QHD includes $\langle \hat{Q}^2 \rangle$, $\langle \hat{P}^2 \rangle$ and the symmetrized cross-term $\langle \hat{P} \hat{Q} \rangle_s$. The higher order variables are approximated by the products of the first and second moments [81, 83, 84], Eq. (2). The QHD-2 EOM conserve the total energy as well as the Heisenberg uncertainty

$$\left(\langle \hat{P}^2 \rangle - \langle \hat{P} \rangle^2 \right) \left(\langle \hat{Q}^2 \rangle - \langle \hat{Q} \rangle^2 \right) - \left(\langle \hat{P} \hat{Q} \rangle_s - \langle \hat{P} \rangle \langle \hat{Q} \rangle \right)^2 = C. \quad (10)$$

The latter can be used [85] to eliminate one of the five variables and define the four new variables

$$q = \langle \hat{Q} \rangle, \quad p = \langle \hat{P} \rangle, \quad (11)$$

$$s = \sqrt{\langle \hat{Q}^2 \rangle - \langle \hat{Q} \rangle^2}$$

$$p_s = m \frac{ds}{dt} = \frac{\langle \hat{P} \hat{Q} \rangle_s - \langle \hat{P} \rangle \langle \hat{Q} \rangle}{\sqrt{\langle \hat{Q}^2 \rangle - \langle \hat{Q} \rangle^2}}$$

such that the QHD-2 EOM obtained by the closure of the Heisenberg hierarchy become equivalent to the classical Hamiltonian EOM for the following Hamiltonian [85, 103]

$$H(p, q, p_s, s) = \frac{p^2 + p_s^2}{2m} + V(q) + \frac{1}{2} V^{(2)}(q) s^2 + \frac{1}{8} V^{(4)}(q) s^4 + \frac{\hbar^2}{8ms^2}, \quad (12)$$

where, to be specific, the minimal uncertainty $C = (\hbar/4)^2$ is assumed. With this change of variables, QHD-2 can be understood as classical dynamics in doubled dimensions.

3.2 Example: escape from a metastable state

The cubic potential (5) represents the simplest case requiring a closure and describes tunneling escape from a metastable state. The two-dimensional effective classical potential (12) of mapped QHD-2 corresponding to the cubic potential (5) is plotted in Fig. 1a. Two features arising from the extra dimension facilitate the escape. First, the floor of the potential is

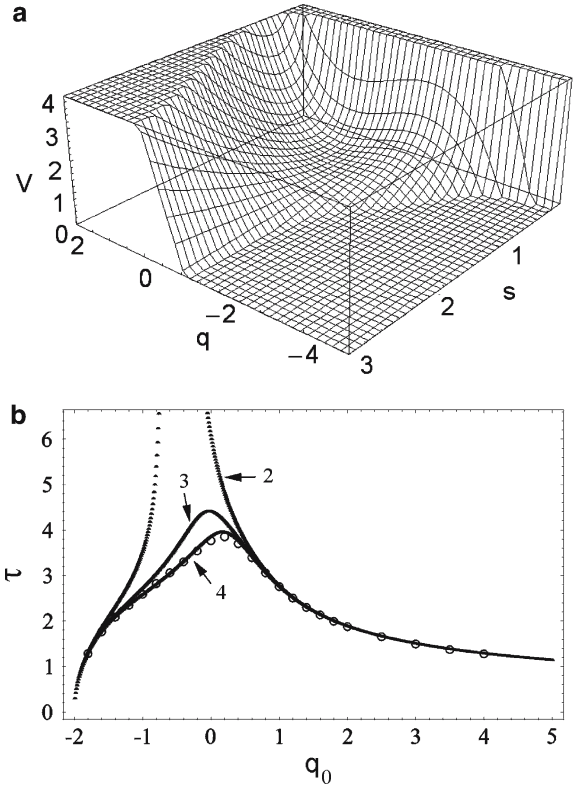


Fig. 1 **a** Representation of the cubic potential (5) in the double-dimensional space of mapped QHD-2, Eq. (12). **b** Barrier crossing times for a particle initially centered at q_0 . Classical particles starting within $-2 < q_0 < 1$ remain trapped indefinitely. Shown are the exact quantum results (circles) and the QHD results at the second, third and fourth order

raised above zero by the combination of the s^2 and $1/s^2$ terms in (12) that represent the potential and kinetic energy contributions to ZPE. The $1/s^2$ term is also responsible for keeping the width s positive at all times. Second, expansion in the width dimension creates a lower-energy saddle point relative to the top of the classical barrier. The tunneling time can be interpreted in QHD as the time the trajectory takes to locate the saddle point in the extra dimension, with the original barrier responsible for creating a bottleneck for the dynamics in the extended phase space.

Figure 1b shows the results for the classically forbidden decay of a particle of unit mass prepared in the ground state of the harmonic potential $\hat{Q}^2/2$. One can think of a vibrational wave packet in the harmonic ground electronic state that is promoted into the metastable excited electronic state. The ground-state Gaussian wavepacket has been shifted to q_0 and allowed to evolve with zero initial momentum. The wavepacket corresponding to the first vibrational excited state is considered in [84]. Figure 1b plots the time at which the center q of the wavepacket crosses the top of the barrier. The exact quantum results are shown by the circles. The QHD-2, 3 and 4 data are indicated by the arrows. The barrier is located at $q = -2$, such that a classical particle starting between $-2 < q_0 <$

1 with zero kinetic energy remains indefinitely trapped. The QHD-2 results approximate the quantum-mechanical behavior very well for $-2 < q_0 < -1.4$ and $0.6 < q_0 < -1$. QHD-4 converges to the exact data. Although a classical mapping is not known for higher order QHDs, the potential energy can still be investigated. The cubic potential is treated exactly in QHD-3. Considered as a function of the first three moments of \hat{Q} , the cubic potential has no barrier that can prevent the particle escape. Tunneling becomes a purely dynamical effect of finding the escape route. The deviations between the exact and QHD-3,4 results are present because the exact quantum dynamics in a cubic potential involves all orders of \hat{P} and \hat{Q} .

3.3 Example: vibrational energy flow between the OH stretches in water

The second moments of \hat{P} and \hat{Q} represent the harmonic energy and make QHD-2 well suited for the treatment of ZPE and vibrational energy exchange. In contrast to classical mechanics, which does not preserve ZPE and misrepresents the energy flow between vibrational modes, QHD-2 globally preserves ZPE and more closely matches the quantum vibrational energy flow, as illustrated by the energy exchange between the OH stretching modes of water [83]. The SPC-flexible model of water [104, 105], a standard model in classical molecular dynamics that provides good description of both molecular and bulk properties, represents the OH stretches as bilinearly coupled Morse oscillators

$$V(q_1, q_2) = D \left[(1 - e^{-\alpha q_1})^2 + (1 - e^{-\alpha q_2})^2 \right] + K q_1 q_2. \quad (13)$$

The parameters are given in Table 1. The OH stretching frequencies are around $3,000 \text{ cm}^{-1}$, such that the quantum ZPE significantly exceeds room temperature, since 300 K corresponds to 200 cm^{-1} . The relevant part of the Morse potential is shown in Fig. 2a, together with the two lowest eigenstates and the Taylor expansion used in the QHD calculations.

Figure 2b describes the vibrational dynamics that follows the initial displacement of one of the O–H bonds by 0.05 \AA . Shown is the harmonic energy stored in the mode that was not displaced. The quantum and QHD-2 calculations were started with the ground state of the shown mode and the shifted ground state of the displaced mode. The classical data were obtained by position and momentum averaging over the Wigner distribution corresponding to the quantum initial conditions. The computational effort of the QHD calculation was only twice that of a single classical trajectory and orders of magnitude smaller than the efforts of the classical ensemble and quantum simulations. At minimal expense,

Table 1 Parameters of the coupled Morse oscillators representing the OH stretches of water, Eq. (13)

m	m_H
D	0.708 mdyn \AA
α	2.567 \AA^{-1}
K	$0.776 \text{ mdyn \AA}^{-1}$

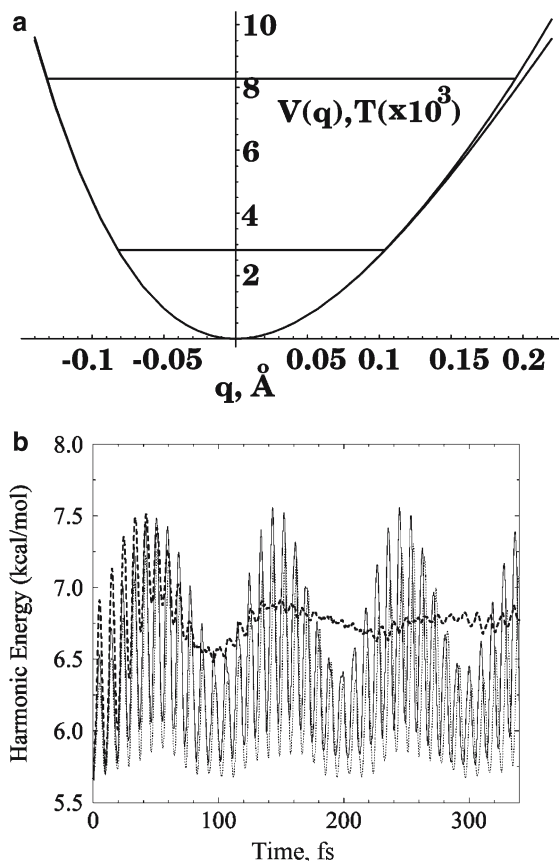


Fig. 2 **a** The Morse potential representing the OH stretch of water. Shown are the two lowest energy levels and the Taylor expansion used in the quantized Hamilton dynamics (QHD) calculations. **b** Energy stored in the OH bond coupled to the other bond that has been initially displaced by 0.05 \AA . Shown are the exact quantum (solid line), classical (dashed line) and QHD-2 (dotted line) results

QHD-2 closely follows the exact quantum dynamics for a long time. Classical mechanics is only able to reproduce the first few oscillations.

3.4 Example: double-slit interference

QHD-2 in moments of \hat{P} and \hat{Q} is ideally suited for ZPE and can describe moderate tunneling. Surprisingly, it can also describe quantum interference, although qualitatively. Consider the double-slit experiment represented by the two-dimensional surface

$$V(x, y) = \left(V_0 - \frac{1}{2} m \omega^2 y^2 + \frac{m^2 \omega^4 y^4}{16 V_0} \right) e^{-(x/\alpha)^2}. \quad (14)$$

The potential is flat for large x and has a double minimum in the y -direction near the origin, Fig. 3a. The parameters have the following values: $\alpha=50 \text{ a.u.}$, $\omega=600 \text{ cm}^{-1}$, $V_0=8,000 \text{ cm}^{-1}$; the particle has the mass of electron [106]. In the simplest QHD the x -coordinate is treated classically, while the

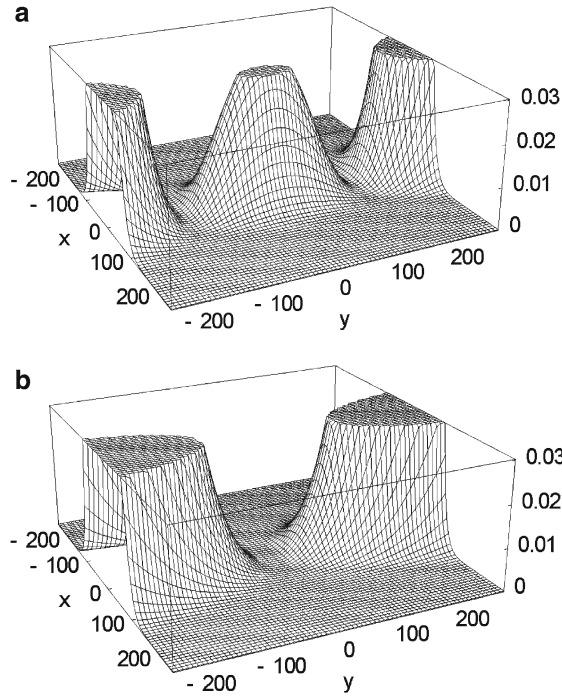


Fig. 3 The effective QHD-2 potential in the double-slit experiment experienced by **a** narrow classical-like particle and **b** particle with the width of 100 a.u., on the order of the distance between the slits

double-slit coordinate y is augmented with the second moment of \hat{Q} creating the effective potential

$$V(x, y; s_y) = V(x, y) + \frac{1}{2} \frac{\partial^2 V(x, y)}{\partial y^2} s_y^2 + \frac{\hbar^2}{8ms_y^2} \quad (15)$$

that parametrically depends on the particle width s_y in the y -dimension, cf. Eq. (12). The constant width approximation obtained [85] from the Heisenberg hierarchy (5) by terminating at the third equation with $\langle \hat{P} \hat{Q} \rangle \approx \langle \hat{P} \rangle \langle \hat{Q} \rangle$ resembles frozen Gaussians [99]. The essential difference from frozen Gaussians, which evolve on the original classical potential (14), is in the second term in (15). The effective potential is shown in Fig. 3a,b for $s_y=1$ and 100 a.u. The $s_y=1$ potential is visually indistinguishable from the classical potential. The $s_y=100$ potential is entirely transformed. Narrow classical-like particles pass through either of the two slits. With increasing width the second term in (15) grows to dominate over the classical potential. Since the second derivative of a quartic potential is a quadratic potential, the double-well in the y direction transforms into a harmonic well. The double-slit becomes a single-slit centered at the origin. As the width continues to increase, the potential remains a single slit approaching the width of $2\sqrt{4V_0/3m\omega^2}$. QHD particles that are wide enough to encompass both slits show interference patterns with a dominant central maximum [86].

4 Coupling of Schrödinger quantum mechanics to QHD

Consider a system composed of light (q) and heavy (Q) particles, such as electrons and nuclei in a molecule. Treating the light subsystem quantum mechanically and the heavy subsystem classically is standard practice. The quantum effects, which are not included in a classical description of the nuclei, can be easily incorporated with QHD. For instance, a quantized mean-field (MF) extension of the quantum-classical Ehrenfest MF has been obtained [82] using the mixed Schrödinger–Heisenberg representation. The interaction part V of the full Hamiltonian

$$\hat{H} = H(\hat{q}, \hat{Q}) = H_1(\hat{q}) + H_2(\hat{Q}) + V(\hat{q}, \hat{Q}), \quad (16)$$

is Taylor expanded in the Q coordinate leading to the following Schrödinger equation for the wave function

$$\begin{aligned} i\hbar \frac{\partial \Psi(q)}{\partial t} &= \langle \chi(Q) | H(\hat{q}, \hat{Q}) | \chi(Q) \rangle \Psi(q) \\ &= \left[H_1(\hat{q}) + V(\hat{q}, \langle \hat{Q} \rangle) + \frac{1}{2} V''(\hat{q}, \langle \hat{Q} \rangle) \right. \\ &\quad \left. \times (\langle \hat{Q}^2 \rangle - \langle \hat{Q} \rangle^2) + \dots \right] \Psi(q). \end{aligned} \quad (17)$$

The light particle is coupled to the MF of the heavy particle represented in the Heisenberg picture by the averages $\langle \hat{Q} \rangle$, $\langle \hat{Q}^2 \rangle$, etc. over the initial wave function $\chi(Q)$. The evolution of the heavy particle is represented by the moments of \hat{Q} and \hat{P} coupled to the MF of the light particle

$$\begin{aligned} i\hbar \frac{d(\langle \hat{Q}^n \hat{P}^m \rangle)}{dt} &= \langle \Psi(q) | \left[\langle \hat{Q}^n \hat{P}^m, H(\hat{q}, \hat{Q}) \right] | \Psi(q) \rangle \\ &= \left[\langle \hat{Q}^n \hat{P}^m, H_2(\hat{Q}) \right] \\ &\quad + \langle \Psi(q) | \left[\langle \hat{Q}^n \hat{P}^m, V(\hat{q}, \hat{Q}) \right] | \Psi(q) \rangle. \end{aligned} \quad (18)$$

The quantized MF approach reduces to the Ehrenfest method when all moments of \hat{P} and \hat{Q} are decomposed to first order. Analogous quasi-classical schemes can be constructed using a multi-configuration MF ansatz, where the coupling between the two subsystems is represented by a linear combination of the MF products.

4.1 Example: a light particle scattering off a surface phonon

The advantages of quantized MF method over Ehrenfest dynamics are illustrated with a model designed as a simplified representation of gaseous oxygen interacting with a platinum surface [107,78]. The system consists of a light particle of mass m colliding with a heavier particle of mass M , which is bound to an immobile surface. The interaction potentials are

$$\begin{aligned} V_1(q) &= a[e^{-2b(q-c)} - 2e^{-b(q-c)}], \\ V_2(Q) &= \frac{1}{2} M \Omega^2 Q^2, \\ V(q, Q) &= A e^{-B(q-Q)} \end{aligned} \quad (19)$$

Table 2 Parameters of the light particle scattering off the surface phonon, Eq. (19)

m	1 amu	a	700 kJ/mol
M	10 amu	b	5.0 Å ⁻¹
Ω	4 × 10 ¹⁴ s ⁻¹	c	0.7
A	10 ⁴ kJ/mol	q ₀	6.0 Å
B	4.25 Å ⁻¹	γ	0.5 Å

with the parameters provided in Table 2. Initially, the light particle is moving towards the heavy particle and is described by a Gaussian of width γ located 6 \AA away from the surface. The initial momentum $k_0 = -\sqrt{2mE_0}$ is determined by the incident energy E_0 . At time zero, the heavy particle is in the harmonic oscillator ground state. The following EOM are employed

$$\begin{aligned}
 i\hbar \frac{\partial \Psi(q)}{\partial t} &= \left[T_1(\hat{q}) + V_1(\hat{q}) + V(\hat{q}, \langle \hat{Q} \rangle) \right] \Psi(q) \\
 \frac{d\langle \hat{Q} \rangle}{dt} &= \frac{\langle \hat{P} \rangle}{M} \\
 \frac{d\langle \hat{P} \rangle}{dt} &= -M\Omega^2 \langle \hat{Q} \rangle - \langle \Psi(q) | V'(\hat{q}, \langle \hat{Q} \rangle) | \Psi(q) \rangle \\
 \frac{d\langle \hat{Q}^2 \rangle}{dt} &= \frac{2\langle \hat{P} \hat{Q} \rangle_s}{M} \\
 \frac{d\langle \hat{P} \hat{Q} \rangle_s}{dt} &= \frac{\langle \hat{P}^2 \rangle}{M} - M\Omega^2 \langle \hat{Q}^2 \rangle - \langle \hat{Q} \rangle \langle \Psi(q) | V'(\hat{q}, \langle \hat{Q} \rangle) | \Psi(q) \rangle \\
 \frac{d\langle \hat{P}^2 \rangle}{dt} &= -2M\Omega^2 \langle \hat{P} \hat{Q} \rangle_s - 2\langle \hat{P} \rangle \langle \Psi(q) | V'(\hat{q}, \langle \hat{Q} \rangle) | \Psi(q) \rangle.
 \end{aligned} \tag{20}$$

The Taylor expansion of the interaction potential is intentionally truncated at the first order, such that the equations may be easily implemented with *ab initio* electronic structure codes that often stop at the first derivative. The light-heavy coupling is described by maximally decomposing the terms of the type $\langle \chi(Q)\Psi(q) | \hat{P} V'(\hat{q}, \hat{Q}) | \Psi(q)\chi(Q) \rangle$. The first three equations in (20) are equivalent to the Ehrenfest approach and are independent of the last three equations, because the quasi-classical subsystem is harmonic. The difference from the Ehrenfest approach enters in the initial conditions for the heavy particle. The QHD initial conditions are computed as the expectation values of the relevant operators over the heavy particle's wavefunction. Classically, the initial conditions for P and Q are sampled from the Wigner transform of the wavefunction, generating an ensemble of Ehrenfest trajectories. The classical sampling is needed to represent ZPE of the heavy particle [108]. In QHD, ZPE is stored in the second order variables.

The results of the simulation are characterized by the scattering probability of the light particle

$$P_s(t) = \int_{q_s}^{\infty} |\Psi(q, t)|^2 dq \tag{21}$$

with $q_s \approx 5.8 \text{ \AA}$. All approaches agree at high incident energies. Disagreement occurs at lower energies, as illustrated

in Fig. 4. The Ehrenfest data differ from the exact quantum results at both short and long times. At short times, the Ehrenfest scattering probability grows too rapidly relative to the quantum scattering probability. The energy of the heavy particle is fully available for exchange with the light particle, since ZPE is not preserved. As a result of the excess energy transfer from the heavy to the light particle during the early evolution, the heavy particle is left with insufficient energy to continue promoting the scattering of the light particle at longer times. These problems are resolved by the quantized MF approach [82].

5 QHD equations for a spin-phonon system

The QHD formalism developed above with the hierarchy of moments of \hat{P} and \hat{Q} can be applied to any relevant operators, providing a reduced description of the problem in hand. Quantum phenomena such as coherent excitation transfer, dephasing, branching, and state-specific dynamics can be more effectively described with a Marcus-type model, where donor and acceptor quantum states are coupled to a continuum of bath states. Deeper tunneling in a double-well, for instance, can be captured by extending QHD to higher orders in \hat{P} and \hat{Q} or, more efficiently, by mapping the problem onto a two-level donor-acceptor system coupled to a harmonic oscillator.

The Jaynes-Cummings Hamiltonian [109]

$$H_{JC} = \omega (a^+ a + 1/2) + \Omega S_+ S_- + g (a^+ S_- + a S_+) \tag{22}$$

constitutes a well-known spin-phonon model that captures many key features of molecular systems and is a special case of the Marcus model [88]. The first term in (22) describes a phonon of frequency ω . The second term represents a spin-1/2 particle with energy gap Ω . S_+ , S_- and a^+ , a are the raising and lowering operators of the spin and phonon subsystems, respectively. The last term gives the spin-phonon coupling in the rotating wave, or resonance approximation, where loss of a phonon quantum is accompanied by a gain of a spin quantum and vice versa. The model can be interpreted as that of a molecular dimer undergoing energy transfer mediated by an intermolecular mode [88]. The exact solution to the problem can be obtained in the form of an infinite series [109]. The dynamics driven by the Jaynes-Cummings Hamiltonian is analyzed below with the QHD formalism which provides a very simple and accurate approximate solution and is applicable to a multi-state/multi-mode case.

5.1 Example: population transfer and dephasing

Consider the evolution of the spin variable S_z that describes the difference in the populations of the two states and represents the reaction coordinate for exciton, electron, and proton transfer as well as other chemical processes. The coupling to the phonon induces dephasing in the population transfer. The time-derivative (1) of $S_z = (S_+ S_- - S_- S_+)/2$ initiates an

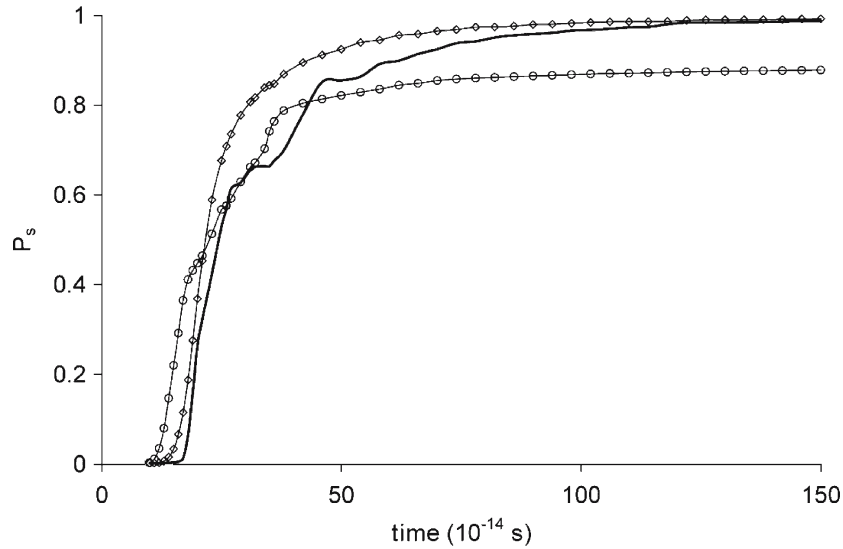


Fig. 4 The time dependent scattering probability of the light particle colliding with the surface phonon computed exactly (*solid line*), by the Ehrenfest (*circles*) and quantized (*diamonds*) mean-field methods

infinite hierarchy of EOM that can be written in a compact form using the non-interacting Hamiltonian γ , the interaction α , and the auxiliary operator β

$$\begin{aligned}\alpha &= a^+ S_- + a S_+, \\ \beta &= a^+ S_- - a S_+, \\ \gamma &= a^+ a + S_+ S_- + \frac{1}{2}.\end{aligned}\quad (23)$$

The Heisenberg hierarchy

$$\begin{aligned}i \frac{d}{dt} \langle S_z \gamma^n \rangle &= g \langle \beta \gamma^n \rangle, \\ i \frac{d}{dt} \langle \alpha \gamma^n \rangle &= -\delta \langle \beta \gamma^n \rangle, \\ i \frac{d}{dt} \langle \beta \gamma^n \rangle &= -\delta \langle \alpha \gamma^n \rangle + g \underbrace{\langle S_z \gamma^{n+1} \rangle}_{\text{needs closure}},\end{aligned}\quad (24)$$

with $n = 0, 1, 2, \dots$ and detuning $\delta = \Omega - \omega$, is arranged in blocks of three equations and a coupling term between the n and $n + 1$ order blocks. Approximations to the hierarchy are obtained in the QHD formalism by closure. To second order, cf. Eq. (2),

$$\langle S_z \gamma^2 \rangle \simeq 2 \langle S_z \gamma \rangle \langle \gamma \rangle + \langle S_z \rangle \langle \gamma^2 \rangle - 2 \langle S_z \rangle \langle \gamma \rangle^2. \quad (25)$$

While closures typically give non-linear equations, such as the classical Hamilton EOM, the second order QHD approximation to (24) with $n = 0, 1$ yields a system of six coupled linear differential equations, since the γ and γ^2 terms appearing in the closure (25) are integrals of motion of the Hamiltonian (22). The equations can be solved for $\langle S_z \rangle$

$$\begin{aligned}\langle S_z \rangle(t) &= \langle S_z \rangle(0) + \frac{\omega_+^2 - \delta^2}{4\omega_+^2} (1 - \cos \omega_+ t) \\ &\quad + \frac{\omega_-^2 - \delta^2}{4\omega_-^2} (1 - \cos \omega_- t),\end{aligned}\quad (26)$$

where $\gamma_0 = \langle \gamma \rangle_{t=0}$ and $\omega_{\pm}^2 = \delta^2 + 2g^2 (\gamma_0 \pm \sqrt{\gamma_0})$. $\langle S_z \rangle$ evolves by a superposition of the two oscillations, whose frequencies differ in proportion to the square of the spin-phonon coupling constant g and the square root of the number of vibrational $a^+ a$ quanta in γ , Eq. (23). Fig. 5a compares the approximate $\langle S_z \rangle$ with the exact quantum result for the following parameters $g = 0.25$, $\delta = 0$ and initial conditions $\langle S_z \rangle_{t=0} = -1/2$, $\langle \gamma \rangle_{t=0} = \langle a^+ a \rangle_{t=0} = 49$, $\langle \alpha \rangle_{t=0} = \langle \beta \rangle_{t=0} = 0$. The sum of the cosine functions in (26) produces beats. The faster oscillation gives the population transfer, while the slower frequency reflects the vibrationally-induced dephasing. The approximate QHD solution correctly reproduces both the population transfer and dephasing over several forward and backward reaction steps.

5.2 Example: Coherence transfer and state-specific dynamics

The evolution of the phonon coordinate $q = \sqrt{2}\text{Re}[a]$ does not explicitly enter the hierarchy (24) and initiates a separate hierarchy

$$\begin{aligned}i \frac{d\langle a \rangle}{dt} &= -\omega \langle a \rangle - g \langle S_- \rangle, \\ i \frac{d\langle S_- \rangle}{dt} &= -\Omega \langle S_- \rangle + 2g \langle a S_z \rangle, \quad \dots\end{aligned}\quad (27)$$

Transformed to the interaction representation $\tilde{a} = a e^{-i\omega t}$, $\tilde{S}_- = S_- e^{-i\Omega t}$, these equations simplify to

$$i \frac{d\langle \tilde{a} \rangle}{dt} = -g \langle \tilde{S}_- \rangle, \quad i \frac{d\langle \tilde{S}_- \rangle}{dt} = 2g \langle \tilde{a} S_z \rangle, \quad \dots\quad (28)$$

The two first-order differential equations are equivalent to a single second-order differential equation

$$\frac{d^2}{dt^2} \langle \tilde{a} \rangle - 2g^2 \langle \tilde{a} S_z \rangle = 0. \quad (29)$$

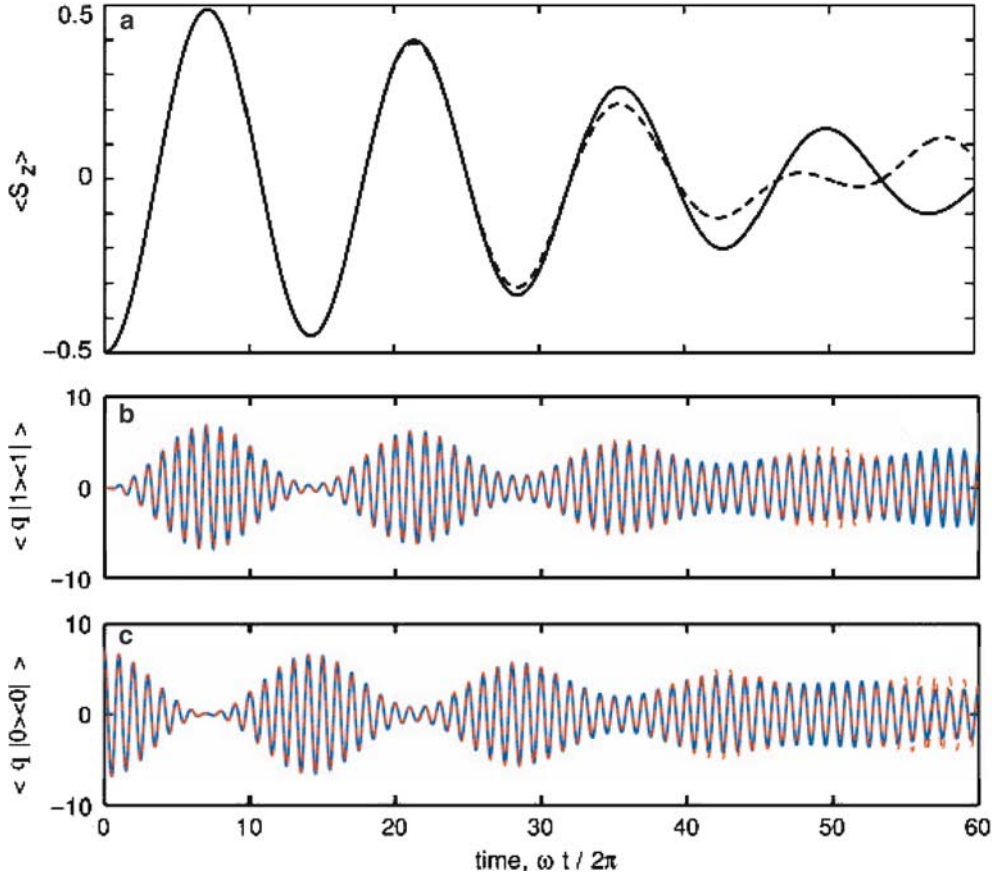


Fig. 5 **a** The population transfer and its dephasing induced by coupling to a phonon in the Jaynes-Cummings model, computed exactly (*solid line*) and with QHD-2 (*dashed line*). **b, c** The state-specific vibrational coordinates showing repeated vibrational coherence transfer between the states

The spin–phonon correlation is approximated by the first order closure

$$\langle \tilde{a} S_z \rangle \simeq \langle \tilde{a} \rangle \langle S_z \rangle, \quad (30)$$

relating to the earlier result (26) for $\langle S_z \rangle$. Equation (29) can be solved numerically. Physically important conclusions can be derived from the approximate perturbative solutions controlled by the spin–phonon coupling constant g .

Spectroscopic experiments usually deal with state-specific rather than average properties, since the donor and acceptor states usually obey different selection rules and are probed independently. The state-specific vibrational dynamics shows non-trivial quantum signatures and vibrational coherence transfer in the recent pump-probe experiments [110–113]. The vibrational coordinate associated with state $|i\rangle$ is defined using the projection on this state $|i\rangle\langle i|$

$$\begin{aligned} \langle q|0\rangle\langle 0| &= \langle q \hat{1}/2 + q S_z \rangle \simeq \langle q \rangle (1/2 + \langle S_z \rangle) \\ \langle q|1\rangle\langle 1| &= \langle q \hat{1}/2 - q S_z \rangle \simeq \langle q \rangle (1/2 - \langle S_z \rangle), \end{aligned} \quad (31)$$

with $\hat{1} = |1\rangle\langle 1| + |0\rangle\langle 0|$ and $S_z = (|1\rangle\langle 1| - |0\rangle\langle 0|)/2$. The approximate results constructed using Eqs. (26), (29), and (30) show excellent agreement with the exact quantum calculations (Fig. 5b,c).

The coupled electron–phonon dynamics forms a hierarchy of time scales associated with distinct physical processes. The quickest time $t_I \sim \omega$ is due to the oscillation of the vibrational coordinate $\langle q \rangle$ and electronic coherence $\langle S_x \rangle, \langle S_y \rangle$. The second time scale $t_{II} \sim g\sqrt{2}\langle \gamma_0 \rangle$ characterizes the inversion of the state population $\langle S_z \rangle$. Dephasing of the population inversion occurs on a slower time scale $t_{III} \sim g/\sqrt{2}$. The slowest component $t_{IV} \sim g/\sqrt{\langle \gamma_0 \rangle}$ is associated the revival of the oscillation of $\langle S_z \rangle$. The simple QHD treatment of the problem accurately reproduces the three fastest time scales. The revival is generated by a superposition of multiple frequencies available in the exact quantum solution, but not accessible in the reduced description. The QHD treatment, however, can be easily applied to a multi-state, multi-phonon generalization of the problem, where revivals are not expected even at the classical level. The approximation described above is significantly superior to the Ehrenfest method, which fails to describe the population dephasing and excludes any state-specific information.

6 Thermal averaging in QHD

It is desirable for many reasons to be able to address both dynamical and statistical mechanical aspects of a problem

at the same time. Most experimental signals are Boltzmann averaged. Dynamical trajectories in classical mechanics are often used to obtain statistical averages. Dynamical fluctuations in equilibrium are related to linear response coefficients. It is not trivial to establish a proper statistical averaging over the extended space of QHD variables, or to relate the dynamics to the statistics. All states sampled by an ergodic trajectory contribute to the statistical sum in classical mechanics. In contrast, a quantum statistical sum involves linearly independent basis states, while quantum dynamics covers arbitrary superpositions of states. The discrepancy between the statistical and dynamical sets of states in quantum mechanics manifests itself in QHD, as discussed below for the mapped second order QHD, Eq. (12).

6.1 Boltzmann integration in the second order QHD

Consider a harmonic oscillator at temperature T which has a classical thermal energy of $k_B T$. The QHD-2 harmonic oscillator mapped onto classical mechanics with doubled dimensionality, Eq. (12), is described by the Hamiltonian

$$H_{\text{HO}} = \frac{p^2}{2m} + \frac{p_s^2}{2m} + \frac{kq^2}{2} + \frac{ks^2}{2} + \frac{\hbar^2}{8ms^2}. \quad (32)$$

The classical Boltzmann averaging in the extended phase space gives the average energy of $2kT + \hbar\omega/2$, preserving ZPE, but adding an extra kT from the quantum dimension. Omitting the quantum dimension from the averages [114, 115] leads to $\hbar\omega/2 + kT$, which is not exact, but gives ZPE and the correct temperature dependence. For a general potential however, the quantum s and classical q are coupled, and the s dimension cannot be separated and dropped.

A solution suggested in [89] reconsiders the thermodynamic connection for the statistical mechanical Lagrange multiplier $\beta = 1/k_B T$ [116]. In mapped QHD-2, the canonical partition function Q for an ensemble of N indistinguishable free particles in a three dimensional box with sides L is

$$Q = \frac{1}{N!} \left[\int_{-\infty}^{\infty} dp \int_0^L dq \int_{-\infty}^{\infty} dp_s \int_0^L ds \times \exp \left[-\frac{\beta'}{2m} \left(p^2 + p_s^2 + \frac{\hbar^2}{4s^2} \right) \right] \right]^{3N}, \quad (33)$$

where β' is the Lagrange multiplier to be determined from thermodynamics. The partition function can be found analytically and, in the classical limit of small \hbar , large m , or small β' , is given by

$$Q = \frac{1}{N!} \frac{8m^{3N} \pi^{3N} V^{2N}}{\beta'^{3N}}, \quad (34)$$

where $V = L^3$. The relationship between the thermodynamic pressure and the partition function can now be used, $P = (1/\beta')(\partial \ln Q / \partial V) = (1/\beta')(2N/V)$. The connection to the ideal gas law $PV = Nk_B T$ gives

$$\beta' = \frac{2}{k_B T}. \quad (35)$$

The factor of 2 difference from the usual relationship appears due to the doubled dimensionality of the mapped QHD-2.

The Boltzmann integration for the QHD-2 harmonic oscillator (32) gives the average energy

$$\langle E_{\text{HO}} \rangle = \frac{\hbar\omega}{2} + \frac{\hbar\omega}{e^{\hbar\omega/k_B T} - 1}. \quad (36)$$

Connection to the exact quantum result yield

$$\beta' = \frac{2}{\hbar\omega} \left(e^{\hbar\omega/k_B T} - 1 \right), \quad (37)$$

which coincides with (35) in the high temperature limit. The frequency ω is not uniquely defined for more general potentials. At low energies most potentials that are used to describe atomic motions may be approximated by a harmonic potential. Since other frequencies become significant only at higher temperatures, when regions of the potential outside the harmonic minimum become energetically accessible, it is reasonable to assign a thermally-averaged frequency for use in Eq. (37):

$$\omega^2 = \frac{\int_{-\infty}^{\infty} (1/m)(d^2V(q)/dq^2) \exp[-\beta V(q)] dq}{\int_{-\infty}^{\infty} \exp[-\beta V(q)] dq}. \quad (38)$$

This average is computed in the usual classical way. Equations (37) and (38) were tested with a series of quartic potentials and gave good agreement with the quantum results, providing a substantial improvement over classical mechanics at low and intermediate temperatures [89]. Figure 6 illustrates this prescription for the Morse potential (13) describing the OH stretch of water [104]. The above procedure is particularly useful in practice, since it can be easily implemented in a general multi-dimensional case with the standard classical molecular dynamics or Monte Carlo techniques.

6.2 QHD coupled to classical bath

An alternative approach has been taken in [90] by closure of the quantum Langevin equation [117]

$$\frac{dY}{dt} = \frac{i}{\hbar} [H_{\text{sys}}, Y] - \frac{i}{2\hbar} \left[F(t) - \gamma \frac{dQ}{dt}, [Q, Y] \right]_+ \quad (39)$$

Application to the first and second moments of \hat{P} and \hat{Q} with $H_{\text{sys}} = P^2/2m + V_{\text{sys}}(Q)$ gives

$$\begin{aligned} \frac{dQ}{dt} &= \frac{P}{m}, \quad \frac{dP}{dt} = \frac{i}{\hbar} [V_{\text{sys}}, P] + F - \gamma P \\ \frac{dQ^2}{dt} &= \frac{2(PQ)_s}{m}, \\ \frac{dP^2}{dt} &= \frac{i}{\hbar} [V_{\text{sys}}, P^2] + 2(PF)_s - 2\gamma P^2 \\ \frac{d(PQ)_s}{dt} &= \frac{i}{\hbar} [V_{\text{sys}}, (PQ)_s] + \frac{P^2}{m} + (QF)_s - \gamma(PQ)_s. \end{aligned} \quad (40)$$

Here, F is noise and γ is friction. The difficulty lies in the interpretation of the noise operator and its products with

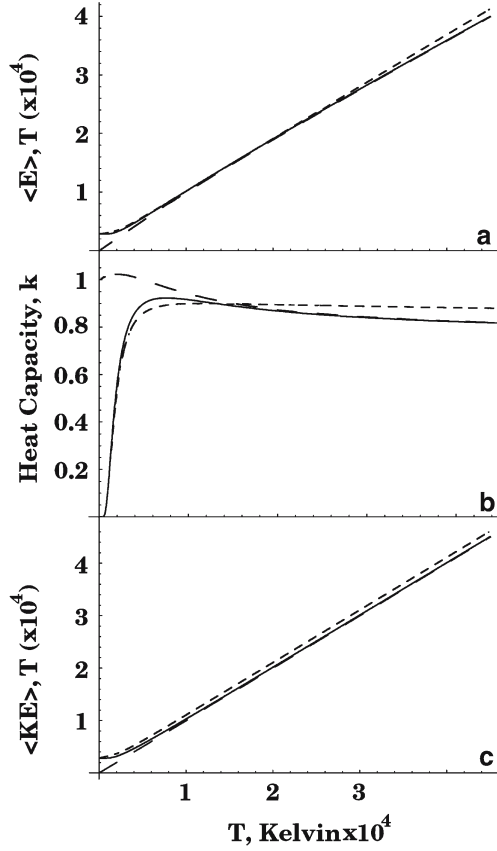


Fig. 6 Thermal averages of (a) total energy, (b) heat capacity and (c) kinetic energy of the OH stretch of water represented by the Morse potential, Fig. 2a, obtained by the modified Boltzmann averaging (37) over the mapped QHD-2 Hamiltonian (12)

P and Q . Avoiding quantum noise [117], the bath can be interpreted classically by decomposing the noise and friction terms to the first order $\langle QF \rangle_s \simeq \langle Q \rangle \langle F \rangle$, etc., and using the classical fluctuation–dissipation theorem: $\overline{\langle F(t) \rangle \langle F(t') \rangle} = 2mk_B T \gamma \delta(t - t')$ in one dimension, where the overbar denotes averaging over the noise. Application of the second order closure to the system operators and the first order closure to the noise and friction terms allows one to perform the classical mapping (11) resulting in

$$\begin{aligned} \frac{dq}{dt} &= \frac{p}{m}, \\ \frac{dp}{dt} &= - \left[V'(q) + \frac{1}{2} V^{(3)}(q)s^2 + \frac{1}{8} V^{(5)}(q)s^4 \right] + F - \gamma p \quad (41) \\ \frac{ds}{dt} &= \frac{p_s}{m}, \\ \frac{dp_s}{dt} &= - \left[V^{(2)}(q)s + \frac{1}{2} V^{(4)}(q)s^3 \right] + \frac{\hbar^2}{4ms^3}, \end{aligned}$$

which describe dynamics of the classical two-dimensional system (12) with the (q, p) degree of freedom coupled to the classical heat bath. The average thermal energies predicted by Eq. (41) for the free particle and harmonic oscillator equal

$k_B T$ and $k_B T + \hbar\omega/2$, respectively. [89] A general potential creates energy flow from bath to (p, q) to (p_s, s) , raising the issues discussed in the previous section. Equations. (37), (38) provide a practical prescription for thermal sampling within mapped QHD-2. It is expected that a more rigorous procedure will require the use of quantum noise.

7 Conclusions

This paper has described our recent efforts in extending classical mechanics to capture ZPE, tunneling, dephasing, branching and other essential quantum effects with a computational effort suitable for multi-dimensional applications. The approach considers the relevant observables directly, without an attempt to reconstruct the full wave function, and uses a closure approximation to terminate infinite Heisenberg hierarchies and arrive at reduced descriptions, augmenting the classical Hamiltonian dynamics with higher order quantum variables. This quantized Hamilton dynamics approach has been applied to study the tunneling escape from a metastable state, the preservation of ZPE during the energy exchange between the OH stretches of water, the interference in the double-slit experiment, the interaction between the light and heavy particles modeled after an O_2 scattering off a Pt surface, the population transfer, dephasing and state-specific vibrational dynamics in a Marcus-type model. The QHD formalism has been developed for the moments of the classical-like \hat{P} and \hat{Q} , the coupling of these moments to a quantum subsystem described in the Schrödinger picture, the spin–phonon operators and the quantum Langevin equation. The dynamics for the second order QHD for \hat{P} and \hat{Q} has been mapped onto classical dynamics. A Boltzmann statistical averaging in the mapped QHD-2 has been introduced.

The main advantages of the approach include a general and flexible prescription for building simple models of quantum phenomena. The closure approximation can be applied to obtain a reduced description of dynamics for any quantum system represented by an arbitrary Hamiltonian and a set of relevant observables. By performing the closure at a desired level, one can derive schemes of varying accuracy and detail. The approach converges to the exact answer, gives error estimates, and provides a systematic way to improve lower order approximations. The simplest extensions of classical mechanics achieved within the QHD framework are particularly valuable. The new quantum variables introduced in such cases can be given transparent physical meaning, the EOMs can be straightforwardly implemented and the dynamics can be easily analyzed. The limitations of the approach involve the short-time nature of the approximations, the growing complexity of closures with increasing order, and the non-linear classical-like equations. It should be noted however that while the QHD extensions of classical mechanics are exact only at short times, the introduction of new variables captures the essential physics – such as ZPE, dephasing and state-specific dynamics – globally for all times. High order closures can be simplified, for instance, by representing the

high order products purely in terms of the first-order classical terms as proposed originally [81], or even by dropping the high orders altogether. The latter will make the classical-like nonlinear QHD equations linear as they are in quantum mechanics.

The formalism and examples considered here can be easily generalized. Numerical stability of the non-linear equations may become an issue, as noted, for instance, in the multi-dimensional Gaussians, whose width may diverge in condensed phase [102]. Large scale applications of the QHD formalism require development of well-characterized models similar to those of classical molecular dynamics and electronic structure theory that, respectively, rely on well-designed interaction potentials and atomic basis sets. The classical mapping of QHD-2 facilitates this task. While the current efforts focus primarily on the low order extensions of classical mechanics, it is straightforward to derive higher order QHDs that converge to the exact quantum answer [84]. Quantum observables can be systematically expanded, for instance, in Fourier operators or Chebyshev polynomials. The choice of the operator bases and the truncation levels for different dimensions grant the method great flexibility.

Acknowledgements The author is infinitely thankful to his past and present colleagues and co-authors, and in particular to Drs. Yuriy Pereverzev, Elke Pahl, Dmitri Kilin, Craig Brooksby and Eric Heatwole. The New Faculty Award of the Camille and Henry Dreyfus Foundation, the Research Innovation Award# R10246 of the Research Corporation, and the Alfred P. Sloan Fellowship are gratefully acknowledged together with the financial support of the NSF Career Award CHE-0994012, Petroleum Research Fund Awards 65-3732 and 150393, and two grants from the University of Washington Royalty Research Fund.

References

- Zewail AH (1996) *J Phys Chem* 100:12701
- Butler LJ (1998) *Annu Rev Phys Chem* 49:125
- Truhlar DG, Garrett BC, Klippenstein SJ (1996) *J Phys Chem* 100:12771
- Jonsson H (2000) *Annu Rev Phys Chem* 51:623
- Bolhuis PG, Chandler D, Dellago C, Geissler PL (2002) *Annu Rev Phys Chem* 53:291
- Fleming GR (1986) *Annu Rev Phys Chem* 37:81
- Xie XS, Trautman JK (1998) *Annu Rev Phys Chem* 49:441
- Makri N (1999) *Annu Rev Phys Chem* 50:167
- Meyer HD, Worth GA (2003) *Theor Chem Acc* 108:251
- Warshel A (2003) *Annu Rev Biophys Biomol Struct* 32:425
- Redondo A, LeSar R (2004) *Annu Rev Mat Res* 34:279
- Schwartz BJ, Rossky PJ (1994) *J Chem Phys* 101:6917
- Schwartz BJ, Rossky PJ (1994) *Phys Rev Lett* 72:3282
- Prezhdo OV, Rossky PJ (1996) *J Phys Chem* 100:17094
- Schwartz BJ, Bittner ER, Prezhdo OV, Rossky PJ (1996) *J Chem Phys* 104:5942
- Prezhdo OV, Rossky PJ (1997) *J Chem Phys* 107:5863
- Mosyak AA, Prezhdo OV, Rossky PJ (1998) *J Chem Phys* 109:6390
- Mosyak AA, Prezhdo OV, Rossky PJ (1999) *J Mol Struct* 485-486:545
- Tully JC (2000) *Ann Rev Phys Chem* 51:153
- Tully JC, Gomez M, Head-Gordon M (1993) *J Vac Sci Tech A – Vac Surf Films* 11:1914
- Head-Gordon M, Tully JC (1995) *J Chem Phys* 103:10137
- Miller WH (2001) *J Phys Chem A* 105:2942
- Miller WH, Zhao Y, Ceotto M, Yang S (2003) *J Chem Phys* 119:1329
- Yamamoto T, Miller WH (2005) *J Chem Phys* 122:044106
- Ceotto M, Miller WH (2004) *J Chem Phys* 120:6356
- Zhao Y, Yamamoto T, Miller WH (2004) *J Chem Phys* 120:3100
- Guallar V, Gherman BF, Miller WH, Lippard SJ, Friesner RA (2002) *J Am Chem Soc* 124:3377
- Fiete GA, Heller EJ (2003) *Rev Mod Phys* 75:933
- Vanicek J, Heller EJ (2003) *Phys Rev E* 67:016211
- Batista VS, Brumer P (2002) *Phys Rev Lett* 89:143201
- Shapiro EA, Kalinski M, Eberly JH (1998) *Opt Expr* 3:124
- Guian CS, Wyatt RE (2000) *J Chem Phys* 112:3580
- Yu N, Coker DF (2004) *Mol Phys* 102:1031
- Cina JA, Kilin DS, Humble TS (2003) *J Chem Phys* 118:46
- Blinov NV, Roy PN, Voth GA (2001) *J Chem Phys* 115:4484
- Hone TD, Voth GA (2004) *J Chem Phys* 121:6412
- Cui Q, Elstner M, Karplus M (2002) *J Phys Chem B* 106:2721
- Gao JL, Truhlar DG (2002) *Ann Rev Phys Chem* 53:467
- Soudackov A, Hatcher E, Hammes-Schiffer S (2005) *J Chem Phys* 122:014505
- Bittner ER, Karabunarliev S (2003) *Int J Quant Chem* 95:521
- Karabunarliev S, Bittner ER (2003) *Phys Rev Lett* 90:057402
- Stier W, Prezhdo OV (2002) *J Phys Chem B* 106:8047
- Stier W, Prezhdo OV (2003) *Isr J Chem* 42:213
- Stier W, Prezhdo OV (2003) *J Mol Struct (Theochem)* 630:33
- Stier W, Duncan WR, Prezhdo OV (2003) *SPIE Proc* 5223:132
- Stier W, Duncan WR, Prezhdo OV (2004) *Adv Mat* 16:240
- Duncan WR, Prezhdo OV (2005) *J Phys Chem B* 109:365
- Duncan WR, Stier WM, Prezhdo OV (2005) *J Am Chem Soc* 127:7941
- Duncan WR, Prezhdo OV (2005) *J Phys Chem B (in press)*
- Craig CF, Duncan WR, Prezhdo OV (2005) *Phys Rev Lett* 95:163001
- Sun X, Miller WH (1997) *J Chem Phys* 106:6346
- Herman MF, Kluk E (1984) *Chem Phys* 91:27
- Billing GD (2002) *Phys Chem Chem Phys* 4:2865
- Ben-Nun M, Martinez TJ (1998) *J Chem Phys* 108:7244
- Ben-Nun M, Martinez TJ (2000) *J Chem Phys* 112:6113
- Kay KG (1992) *Phys Rev A* 46:1213
- Donoso A, Martens CC (2001) *Phys Rev Lett* 87:223202
- Prezhdo OV, Kisil VV (1997) *Phys Rev A* 56:162
- Kapral R, Ciccotti G (1999) *J Chem Phys* 110:8919
- Sergi A, Kapral R (2003) *J Chem Phys* 119:12776
- Sergi A, Kernan DM, Ciccotti G, Kapral R (2003) *Theor Chem Acc* 110:49
- Prezhdo OV, Brooksby C (2001) *Phys Rev Lett* 86:3215
- Lopreore CL, Wyatt RE (1999) *Phys Rev Lett* 82:5190
- Bittner ER, Wyatt RE (2000) *J Chem Phys* 113:8888
- Wyatt RW, Lopreore CL, Parlant G (2001) *J Chem Phys* 114:5113
- Burghardt I, Moller KB, Parlant G, Cederbaum LS, Bittner ER (2004) *Int J Quant Chem* 100:1153
- Babyuk D, Wyatt RE (2004) *Chem Phys Lett* 400:145
- Burghardt I (2005) *J Chem Phys* 122:094103
- Halliwell JJ (1998) *Phys Rev D* 57:2337
- Prezhdo OV (2000) *Phys Rev Lett* 85:4413
- Gelman D, Kosloff R (2003) *Chem Phys Lett* 381:129
- Prezhdo OV (1999) *J Chem Phys* 111:8366
- Tully JC (1990) *J Chem Phys* 93:1061
- Hammes-Schiffer S, Tully JC (1994) *J Chem Phys* 101:4657
- Bittner ER, Rossky PJ (1995) *J Chem Phys* 103:8130
- Prezhdo OV, Rossky PJ (1998) *Phys Rev Lett* 81:5294
- Hack MD, Truhlar DG (2001) *J Chem Phys* 114:9305
- Sholl DS, Tully JC (1998) *J Chem Phys* 109:7702
- Webster FA, Rossky PJ, Friesner RA (1991) *Comp Phys Comm* 63:494
- Prezhdo OV, Rossky PJ (1997) *J Chem Phys* 107:825
- Prezhdo OV, Pereverzev YV (2000) *J Chem Phys* 113:6557
- Brooksby C, Prezhdo OV (2001) *Chem Phys Lett* 346:463
- Prezhdo OV, Pereverzev YV (2002) *J Chem Phys* 116:4450
- Pahl E, Prezhdo OV (2002) *J Chem Phys* 116:8704
- Prezhdo OV (2002) *J Chem Phys* 117:2995

86. Brooksby C, Prezhdo OV (2003) *Chem Phys Lett* 378:533
87. Prezhdo OV, Brooksby C (2003) *Adv Topic in Theor Chem Phys* 12:339
88. Kilin D, Pereverzev YV, Prezhdo OV (2004) *J Chem Phys* 120:11209
89. Heatwole E, Prezhdo OV (2004) *J Chem Phys* 121:10967
90. Heatwole E, Prezhdo OV (2005) *J Chem Phys* 122:234109
91. Kilin D, Prezhdo OV, Brooksby C (2003) *J. Mol. Struct. (Theochem)* 630:45
92. Wick GC (1950) *Phys Rev* 80:268
93. Wilson S (1984) *Electronic correlation in molecules*. Oxford University Press, Oxford, England,
94. Piecuch P, Kowalski K, Pimienta ISO, Fan P-D, Lodriguito M, McGuire MJ, Kucharski SA, Kus T, Musial M (2004) *Theor Chem Acc* 112:349
95. Bogoliubov NN (1965) *The dynamic theory in statistical physics*. Hindustan, Delhi
96. Kawasaki K (1970) *Ann Phys* 61:1
97. Liboff RL (1990) *Kinetic theory: classical, quantum and relativistic descriptions*. Prentice Hall, Englewood Cliffs, NJ
98. Heller EJ (1996) *J Chem Phys* 64:63
99. Heller EJ (1981) *J Chem Phys* 75:2923
100. Sawada S-I, Metiu H (1986) *J Chem Phys* 84:227
101. Coalson RD, Karplus M (1990) *J Chem Phys* 93:3919
102. Buch V (2002) *J Chem Phys* 117:4738
103. Ando K (2003) *Chem Phys Lett* 376:532
104. Toukan K, Rahman A (1985) *Phys Rev B* 31:2643
105. Anderson J, Ullo JJ, Yip S (1987) *J Chem Phys* 87:1726
106. Gelabert R, Geminez X, Thoss M, Wang H, Miller WH (2001) *J Chem Phys* 114:2572
107. Stromquist J, Gao S (1996) *J Chem Phys* 106:5751
108. Guo Y, Thompson DL, Sewell TD (1996) *J Chem Phys* 104:576
109. Jaynes ET, Cummings FW (1963) *Proc IEEE* 51:89
110. Khalil M, Demirdoven N, Tokmakoff A (2004) *J Chem Phys* 121:362
111. Gruebele M (2004) *J Phys - Cond Mat* 16:R1057
112. Cina JA, Fleming GR (2004) *J Phys Chem A* 108:11196
113. Scheurer C, Mukamel S (2002) *J Chem Phys* 116:6803
114. Corbin N, Singer K (1982) *Mol Phys* 46:671
115. Singer K, Smith W (1986) *Mol Phys* 57:761
116. McQuarrie DA (1976) *Statistical Mechanics*. Harper & Row, New York
117. Gardiner CW, Zoller P (2000) *Quantum noise : a handbook of Markovian and non-Markovian quantum stochastic methods with applications to quantum optics*. Springer Berlin Heidelberg, New York